Results in Chemistry 7 (2024) 101505

Contents lists available at ScienceDirect

Results in Chemistry

journal homepage: www.sciencedirect.com/journal/results-in-chemistry

Physicochemical and textural properties of amino-functionalised mesoporous silica nanomaterials from different silica sources

Josephine Oluwagbemisola Tella [a,b], Kolawole Oluseyi Ajanaku [a,*], Joseph Adeyemi Adekoya [a,*], Rajkumar Banerjee [b,c], Chitta Ranjan Patra [b,c], Srinivas Pavuluri [d], Bojja Sreedhar [e]

[a] Department of Chemistry, College of Science and Technology, Covenant University, Ota 112212, Nigeria
[b] Applied Biology Division, CSIR-Indian Institute of Chemical Technology, Tarnaka, Hyderabad 500007, India
[c] Academy of Scientific and Innovative Research (AcSIR), Ghaziabad 201002, U.P., India
[d] Inorganic and Physical Chemistry Division, CSIR-Indian Institute of Chemical Technology, Tarnaka, Hyderabad 500007, India
[e] Department of Analytical and Structural Chemistry, CSIR-Indian Institute of Chemical Technology, Tarnaka, Hyderabad 500007, India

ARTICLE INFO

Keywords:
Mesoporous silica nanomaterials
Amino-functionalisation
Co-condensation
Post-grafting
Solvent-extraction
Calcination

ABSTRACT

A series of MCM-41 nanomaterials that could serve various scientific applications was synthesised from two silica sources, tetraethyl ortho silicate and sodium silicate. Calcination and solvent extraction were employed as surfactant removal methods, while surface functionalisation was done via co-condensation and post-grafting methods. The synthesised nanomaterials were characterised, and their physicochemical properties were compared using X-ray powder diffraction (XRD), Brunauer Emmett Teller (BET) analysis, Fourier Transform Infra-red spectroscopy (FTIR), Thermogravimetric analysis (TGA), Scanning Electron Microscopy (SEM) and Transmission Electron Microscopy (TEM). The results showed that the surfactant removal and surface functionalisation methods affected the synthesised nanomaterials' 2θ values, d-spacing, and unit cell parameters. However, surfactant removal methods did not affect the morphology of amino-functionalised nanomaterials. Mesoporous silica nanomaterials of specific surface areas (884.0–17.1 m^2/g), pore volumes (1.0–0.1 cm^3/g), pore size diameters (7.2–1.5 nm), and less orderly mesoporous structures were produced with co-condensation and amino functionalisation using both silica sources. These methods can produce mesoporous silica nanostructures with different morphologies for wastewater remediation, catalysis, bio-catalysis, drug delivery, CO_2 capture, indoor air cleaning, bioanalytical sample preparation, and pervaporation membrane improvement.

Introduction

Mesoporous silica nanomaterials (MCM-41), since their discovery in 1992, have been widely used for many scientific applications, which cut across drug delivery, catalysis, and energy, among others, due to their unique features [1,2]. Over the years, these well-ordered hexagonal structured materials with 2–50 nm pore diameters, large surface areas of up to 1000 cm^2/g, tuneable pore sizes, and distinct morphologies have been extensively studied for their biomedical applications [3–7].

MCM-41 nanomaterials are commonly synthesised using sol–gel synthesis, which regulates the porosities and morphologies of nanoparticles by varying their synthesis parameters such as silica precursors, reaction temperature and time, solvents, surfactants, and pH, to mention a few [8]. The use of alkoxide compounds as silica precursors for synthesising mesoporous silica nanoparticles is limited due to environmental and economic reasons (toxicity and high cost of silica source). Silicate precursors such as sodium silicate are economical and non-toxic. Hence, they are preferred and used as a substitute for alkoxide compounds [9].

Surfactants that act as structure-directing agents with varying alkyl chain lengths are used as templates during the synthesis of mesoporous nanoparticles to control their pore structure and sizes [10]. Cetyltrimethylammonium bromide (CTAB), a quaternary ammonium surfactant, has been used to synthesise MCM-41 with notable structural properties [11]. After synthesis, surfactant removal is done to obtain the mesoporous structure and pore network [12]. Surfactant interactions with the nanoparticle's silica framework are also reduced, and surface functionalisation of the nanomaterials with functional groups becomes easier after surfactant removal [13]. Several surfactant removal methods have been employed and reported in the literature, including

* Corresponding authors.
E-mail addresses: kola.ajanaku@covenantuniversity.edu.ng (K.O. Ajanaku), joseph.adekoya@covenantuniversity.edu.ng (J.A. Adekoya).

https://doi.org/10.1016/j.rechem.2024.101505
Received 21 February 2024; Accepted 16 April 2024
Available online 16 April 2024

calcination and acid-solvent extraction [14].

The surface functionalisation of mesoporous silica surfaces with different functional groups has been reported [15]. Silica surfaces are covered with functional groups that attach them to chemical or biological moieties. Amino groups are attached to silica surfaces using amino silanes as coupling agents. One of the commonly used amino-silanes is 3-amino propyl triethoxysilane (APTES), which is economical [16]. The functionalisation of silica precursors with APTES produces amino-functionalized surfaces that are easily affected by their synthetic conditions, such as temperature, reaction time, the concentration of silane, the quantity of water present in the reaction, and the polarity of solvent used [17].

Various morphologies of MCM-41 nano-materials with controllable structural properties have been synthesised by varying the reaction parameters used in their synthesis [18–22]. The effect of surfactant removal methods on the choice of silica source used and surface functionalisation methods employed are also essential factors to be considered in determining the final properties of MCM-41 nano-materials.

This paper aimed to study the effect of surfactant removal methods (calcination and solvent extraction) and surface functionalisation methods (co-condensation and post-grafting) on the physicochemical and textural properties of amino-functionalized MCM-41 nano-materials. Tetra ethyl ortho silicate and sodium silicate were used as silica sources, while ethanol and methanol were employed as solvents for solvent extraction. The synthesised nanomaterials were studied and compared using characterisation techniques: XRD, FTIR, BET, TGA, SEM, and TEM.

Experimental

Materials

Tetraethyl orthosilicate (TEOS) ($C_8H_{20}O_4Si$, 98 %), sodium *meta*-silicate solution (Na_2Si0_3) Sigma-Aldrich, Louis, MO, USA), cetyl-trimethyl ammonium bromide (CTAB) ($C_{19}H_{42}BrN$, 99.9 %), 3-aminopropyltriethoxysilane (APTES) ($C_9H_{23}NO_3Si$, 99 %), sodium hydroxide pellets, toluene, absolute ethanol and methanol were purchased from Sigma-Aldrich, St Louis, MO, USA and used without further purification. Concentrated hydrochloric acid and tetraoxosulphate (VI) acid were purchased from Rankem Ltd, Mumbai, India. Milli Q water (Millipore) was used to synthesise the nanomaterials.

Synthesis of MCM-41 using tetraethyl orthosilicate (TEOS) as silica source

MCM-41 was synthesised according to the procedure described by Huh et al., 2003 [23] with slight modifications. 2 g of CTAB was dissolved in a solution containing 480 g of Milli-Q water and 7 mL of 2 M NaOH in a Teflon bottle. The mixture was stirred, heated, and maintained at a temperature of 80 °C with continuous stirring for 30 min using a magnetic stirrer. A homogenous solution with a pH of 12.36 was obtained. 9.34 g of TEOS was added rapidly sequentially to the homogeneous solution via injection with continuous stirring to get a white precipitate after about 3 mins. The reaction temperature and time were maintained at 80 °C for 2 h. The as-synthesised product was isolated by hot filtration, washed with enough Milli-Q water and ethanol, and dried under vacuum, as shown in Scheme 1.

Removal of surfactant was done by calcination at 550℃ for 6 h, and two different acid solvent extraction methods involving using methanol and ethanol as solvents at room temperature for 15 mins and 60℃ for 6 h. 1 g each of as-synthesised MCM-41 was suspended in a mixture of ethanol (100 ml) and concentrated hydrochloric acid (1 ml). The mixture was stirred at room temperature for 15 mins and 60℃ for 6 h separately using a magnetic stirrer rotating at 700 rpm. The resulting products were filtered, washed with Milli-Q water and ethanol, and dried under vacuum. The purification was repeated using a mixture of methanol (100 ml) and concentrated hydrochloric acid (1 ml) at the same temperature according to Scheme 1. The final products obtained from calcination were denoted as 'MCM-41-Calt'. Products received after acid solvent extraction at room temperature for 15 mins and 60℃ for 6 h using ethanol as solvent (HCl/EtOH) were denoted as MCM-41-

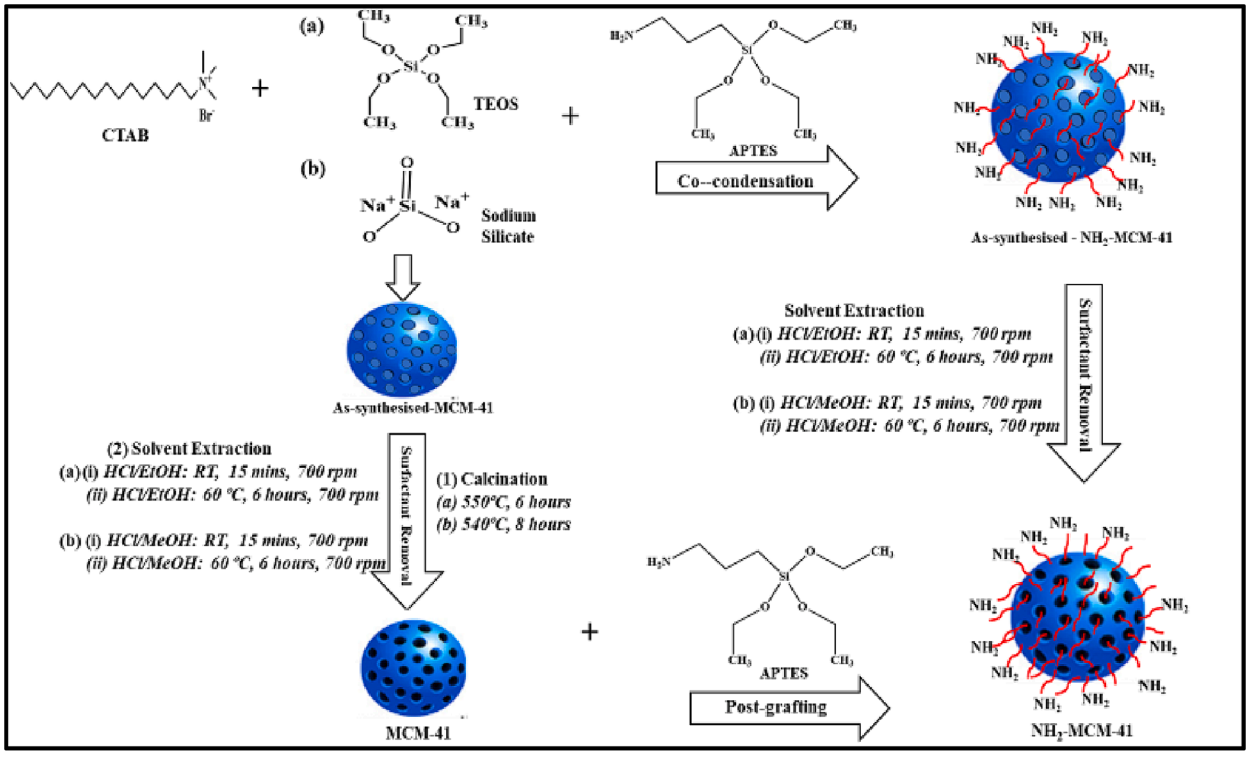

Scheme 1. Illustration of the synthesis of amino functionalised mesoporous silica materials via Co-condensation and post-grafting methods with the surfactant removal methods employed.

Ext1*t* and MCM-41-Ext2*t*, respectively. The products obtained using methanol (HCl/MeOH) as solvent under the same temperature conditions were denoted as MCM-41-Ext3*t* and MCM-41-Ext4*t*, respectively. The calcined and solvent-extracted MCM-41 nanomaterials were prepared as a reference for comparing the amino-functionalised nanomaterials.

Synthesis of amino-functionalised MCM-41 via co-condensation method

Amino-functionalised MCM-41 was synthesised as related in Scheme 1 using a one-pot co-condensation synthesis. The method related to Section 2.2 was adopted. Still, with a drop-wise addition of APTES after the addition of TEOS via injection to make a molar ratio of TEOS/APTES 1:1. The remaining procedure was followed to obtain an as-synthesised product after filtration, washing with enough Milli-Q water and vacuum drying. The surfactant was removed following the acid solvent extraction method described in Section 2.2. The final products obtained were denoted as 'MCM-41-Co1*t*, and MCM-41-Co2*t*' for HCl/EtOH-extracted products and MCM-41-Co3*t* and MCM-41-Co4*t*' for HCl/MeOH-extracted products as earlier stated.

Synthesis of MCM-41 using sodium silicate as silica source

MCM-41 was synthesised according to Scheme 1 using the procedure described by Pauly et al., 2001 [24] with slight modifications. 17.33 g of CTAB was dissolved in 57.5 ml of Milli-Q water and stirred at 700 rpm for 30 mins. 13.45 ml of sodium silicate was added to the homogeneous mixture obtained and stirred for another 30 mins. A 0.667 ml of tetraoxosulphate (VI) acid in 5 ml of Milli-Q water was added to the homogeneous mixture in drops and stirred for 30 mins to obtain a white gel with a pH of 10.3, which was poured into a Teflon bottle and autoclaved for 24 h at 100℃. The resulting gel was washed 4–5 times with Milli-Q water using a centrifuge at 5,000 rpm for 10 mins and then dried in the oven for 12 h at 100℃. Surfactant was removed from the as-synthesised product by calcination (540℃ for 7 h) and acid solvent extraction method as explained in Section 2.2. The final products obtained after calcination and acid solvent extraction were denoted as 'MCM-41-Cal*s*', 'MCM-41-Ext1*s*', 'MCM-41-Ext2*s*', MCM-41-Ext3*s*', and 'MCM-41-Ext4*s*'.

Synthesis of amino-functionalized MCM-41 via co-condensation method

A one-pot co-condensation synthesis, as illustrated in Scheme 1, was carried out using the earlier described method for pure MCM-41 but with a drop-wise addition of APTES following the injection TEOS to make a molar ratio of TEOS/APTES 1:1. When the remaining procedure was followed, an as-synthesised product was obtained after drying in the oven for 12 h at 100℃. The surfactant was removed using the solvent extraction methods related to section 2.2. The final products obtained were 'MCM-41-Co1*s*', 'MCM-41-Co2*s*', 'MCM-41-Co3*s*', and 'MCM-41-Co4*s*'.

Post-grafting synthesis of MCM-41 nanomaterials

The calcined and solvent-extracted MCM-41 was also functionalised as indicated in Scheme 1 through post-grafting synthesis described by Parida and Rath, 2009 [25] with slight modifications. 1 g each of calcined 'MCM-41-Cal*t*' and 'MCM-41-Cal*s*' nanomaterials that were solvent extracted in HCl/EtOH and HCl/MeOH, that is, MCM-41-Ext2*t*, MCM-41-Ext4*t*, MCM-41-Ext2*s*, and MCM-41-Ext4*s* were refluxed separately with 0.785 ml of APTES in 60 ml of toluene for 24 h at room temperature. The product obtained was filtered and washed with Milli-Q water. The resulting products were vacuum-dried and referred to as 'MCM-41-Post-Cal*t*', 'MCM-41-Post-Cal*s*', MCM-41-Post-Ext2*t*, MCM-41-Post-Ext4*t*, MCM-41-Post-Ext2*s*, and MCM-41-Post-Ext4*s*, respectively.

A summary of the nano-materials synthesised in this study with their surfactant removal methods and conditions is presented in Table 1.

Table 1
Summary of synthesised MSNs with their surfactant removal methods and conditions.

	Nano-materials	Surfactant Removal Conditions
1.	MCM-41-Ext1*t* MCM-41-Ext1*s* MCM-41-Co1*t* MCM-41-Co1*s*	• **Method**: Solvent extraction **Temperature:** Room temperature **Stirring time**: 15mins **Stirring rate**: 700 rpm **Solvent used**: HCl/EtOH
2.	MCM-41-Ext2*t* MCM-41-Ext2*s* MCM-41-Co2*t* MCM-41-Co2*s* MCM-41-Post-Ext2*t* MCM-41-Post-Ext2s	• **Method:** Solvent extraction **Temperature:** 60℃ **Stirring time:** 6 h **Stirring rate:** 700 rpm **Solvent used:** HCl/EtOH
3.	MCM-41-Ext3*t* MCM-41-Ext3*s* MCM-41-Co3*t* MCM-41-Co3*s*	• **Method:** Solvent extraction **Temperature:** Room temperature **Stirring time:** 15mins **Stirring rate:** 700 rpm **Solvent used:** HCl/MeOH
4.	MCM-41-Ext4*t* MCM-41-Ext4*s* MCM-41-Co4*t* MCM-41-Co4*s* MCM-41-Post-Ext4*t* MCM-41-Post-Ext4*s*	• **Method:** Solvent extraction **Temperature:** 60℃ **Stirring time:** 6 h **Stirring rate:** 700 rpm **Solvent used:** HCl/MeOH
5.	MCM-41-Cal*t* MCM-41-Post-Cal*t*	• **Method:** Calcination **Temperature:** 550℃ **Time:** 6 h
6.	MCM-41-Cal*s* MCM-41-Post-Cal*s*	• **Method:** Calcination **Temperature:** 540℃ **Time:** 7 h

Surface functionalisation method: Co = co-condensation, Post = post-grafting; Silica source: t = TEOS, s = sodium silicate.

Characterisation

Powder XRD patterns of the synthesised MCM-41 materials were recorded on a Bruker AXS diffractometer (D8 Advance) with a scan 2θ range of 0° to 80° and a scan speed of 1° min^{-1} using filtered CuKα radiation (λ = 1.5406 A°). Particle morphology was analysed with scanning electron microscopy (SEM) using an SEM-ZEISS 1400 scanning electron microscope. TEM images were obtained from JEOL, JEM-2100 Plus Microscope. Fourier transform infrared (FT-IR) spectroscopy was performed on a PerkinElmer-Spectrum GX Spectrometer within the 4000–400 cm^{-1} range using potassium bromide (KBr) pellets. Nitrogen adsorption isotherms of the synthesised nanomaterials were obtained using a NOVA 2200e analyser at −196.15 °C after degassing the samples for 24 hrs at 199.85 °C. TGA analysis was carried out with a Mettler Toledo TGA/SDTA 851e instrument (Zurich, Switzerland) under a nitrogen atmosphere at a 30 ml/min flow rate and temperature of 25 to 800 °C.

Results and discussion

X-ray diffraction studies of synthesised MSNs

The XRD powder patterns of the synthesised nanomaterials for both silica sources are shown in Fig. 1a–d. All the nanomaterials had a single intense diffraction peak with different intensities at plane 100, a typical characteristic of the hexagonal pore structures of MCM-41 materials. This indicates that the nanomaterials retained their mesoporous structure after surfactant removal and amino modification. Weak diffraction peaks corresponding to planes 110 and 200 were also observed in some synthesised nanomaterials. The presence of these peaks implied that the hexagonal pore-structured nanomaterials had well-ordered, long-ranged pores [1,2,26]. At the same time, their absence indicates a decrease or distortion of the pore ordering of the materials because of the surfactant removal method employed and the grafting of amino groups on silica surfaces of the nanomaterials [27–29]. These peaks were more

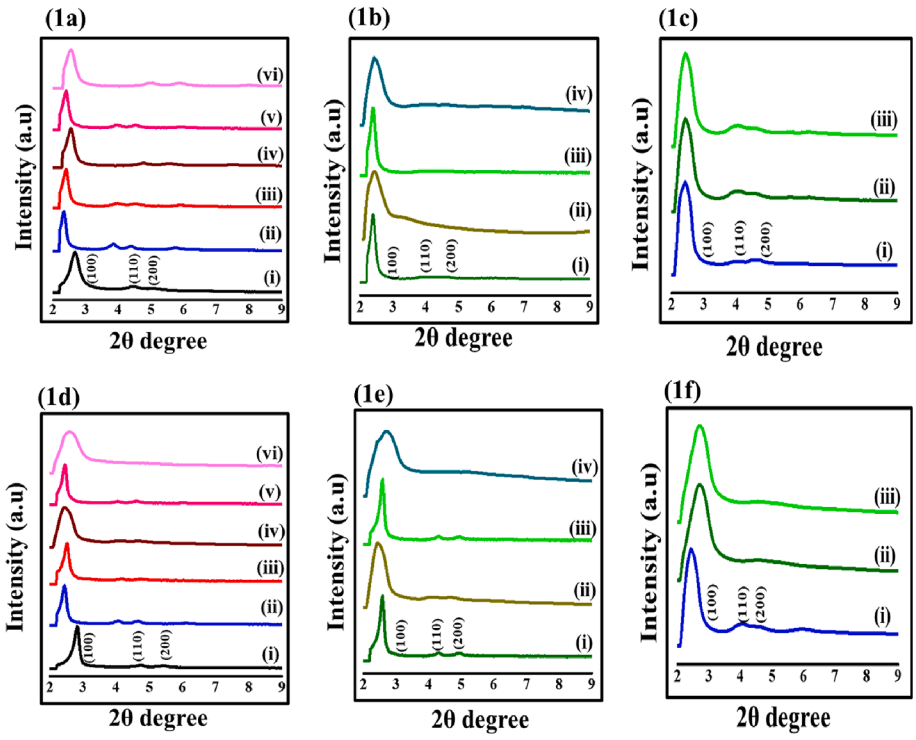

Fig. 1. (a): XRD patterns of MCM-41 nanomaterials synthesised using TEOS as silica source: (i) As-synthesised MCM-41*t*, (ii) MCM-41-Cal*t*, (iii) MCM-41-Ext1*t*, (iv) MCM-41-Ext2*t*, (v) MCM-41-Ext3*t*, (vi) MCM-41-Ext4*t*. **(b):** XRD patterns of co-condensed amino functionalisation MCM-41 nanomaterials synthesised using TEOS as silica source: (i) MCM-41-Co1*t*, (ii) MCM-41-Co2*t*, (iii) MCM-41-Co3*t*, (iv) MCM-41-Co4*t*. **(c):** XRD patterns of post-grafted MCM-41 nanomaterials with TEOS as silica source: (i) MCM-41-Post-Cal*t*, (ii) MCM-41-Post-Ext2*t*, (iii) MCM-41-Post-Ext4*t*. **(d):** XRD patterns of MCM-41 nanomaterials synthesised using sodium silicate as silica source: (i) As-synthesised MCM-41*s*, (ii) MCM-41-Cal*s*, (iii) MCM-41-Ext1*s*, (iv) MCM-41-Ext2*s*, (v) MCM-41-Ext3*s*, (vi) MCM-41-Ext4*s*. **(e):** XRD patterns of co-condensed amino functionalisation MCM-41 nanomaterials synthesised using sodium silicate as silica source: (i) MCM-41-Co1*s*, (ii) MCM-41-Co2*s*, (iii) MCM-41-Co3*s*, (iv) MCM-41-Co4*s*. **(f):** XRD patterns of post-grafted MCM-41 nanomaterials with sodium silicate as silica source: (i) MCM-41-Post-Cal*s*, (ii) MCM-41-Post-Ext2*s*, (iii) MCM-41-Post-Ext4*s*. The supporting dataset can be found at [36]

pronounced in the calcined nanomaterials (MCM-41-Cal*t* and MCM-41-Cal*s*) and less pronounced in nanomaterials that were extracted with HCl/MeOH solvent at 60℃ for 6 h (MCM-41-Ext4*t* and MCM-41-Ext4*s*). They were less orderly than their ethanolic counterparts.

An increase in 2θ values and peak intensities at plane 100 were observed in solvent-extracted non-functionalised nanomaterials (MCM-41-Ext1*t*&*s*, MCM-41-Ext2*t*&*s*, MCM-41-Ext3*t*&*s* and MCM-41-Ext4*t*&*s*) which was due to the shrinkage or sintering of the silica walls after surfactant removal [30,31]. Nanomaterials that were extracted at 60℃ for 6 h in HCl/MeOH solvent (MCM-41-Ext4*t* and MCM-41-Ext4*s*) had slightly higher 2θ values than those extracted in HCl/EtOH solvent at 60℃ for 6 h (MCM-41-Ext2*t* and MCM-41-Ext2*s*).

A decrease in 2θ values and peak intensity was noticed in co-condensed amino-functionalised materials and was more prominent in MCM-41-Co4*t* and MCM-41-Co4*s*. This could be due to amino groups within the mesopores [32,33], which might have caused a decrease in their structural order [34,35]. Co-condensed amino functionalised nanomaterials were observed to have less structural order compared to post-grafted amino functionalised nanomaterials.

Shifts in the 2θ value of diffraction peak (1 0 0) were observed in the nanomaterials, as seen in Table 2. These shifts can be attributed to the structural changes that occurred during surfactant removal and the grafting of amino groups. Inter-planar spacing d_{100} and the hexagonal unit cell parameter (a_o) of the nanomaterials were calculated using the equations $2d\sin\theta = \lambda$ (Bragg's equation) and $2d100\sqrt{3}$, respectively [2].

BET analysis of synthesised MSNs

The nitrogen adsorption/desorption isotherms of the synthesised nano-materials are given in Fig. 2a and b. Fig. 2a(ii), 2a(iii), 2a(iv), 2a (vii), and 2b(ii) isotherms exhibited type IV with hysteresis loops according to IUPAC nomenclature which is typical of mesoporous silica nanoparticles [37]. Transformation in the BET isotherm curves of the parent nano-materials (MCM-41-Cal*t* and MCM-41-Cal*s*) from type IV to type II was observed in some of the nano-materials after surface functionalisation and surfactant removal. This could result from pore blockage caused by amino groups on silica surfaces and the incomplete removal of surfactants from the pores [38,39,40]. The isotherms presented in Fig. 2a(i), (v), (vi), (viii), (ix), (x), (xi), (xii), (xiii) and 2b (i), (iii ~ xiii) can be categorised as type II.

The porosity of the nanomaterials in terms of their specific surface area (S_{BET}), pore size diameter, and volume were determined using nitrogen adsorption–desorption isotherms obtained in Fig. 2a and b. These properties are listed in Table 2. From their specific surface area and pore volumes, BET analysis was used to verify the presence of amino groups in the functionalised nanomaterials and to evaluate the extent of surfactant removal from the nanomaterials. The N_2 adsorption analysis of all the nanomaterials revealed that after grafting with amino groups, a drastic decrease in the surface areas and pore volumes was observed, corresponding with similar literature [25,28]. The decrease was due to amino groups within and on the surface of the mesoporous channels of the nanomaterials.

Co-condensed amino-functionalised materials were observed to have larger specific surface areas compared to post-grafted amino-functionalised nanomaterials. This could be due to the controlled loading and distribution of organic functional groups within and outside the co-condensed materials' silica surfaces, which is difficult to achieve in post-grafted materials [41]. Organic functional groups are mostly

Table 2
Crystallographic parameters observed in synthesised nanomaterials.

No.	Nano-materials Silica source: TEOS	2θ	d_{100} (nm)	a_o (nm)	S_{BET} (m^2/g)	Vp (cm^3/g)	Pore size W_{BJH} (nm)	Pore size W_d (nm)
1	As-synthesised MCM-41 *t*	2.41	3.66	4.23	25.16	0.067	1.05	1.51
2	MCM-41-Cal*t*	2.69	3.28	3.79	860.51	0.606	2.82	2.87
3	MCM-41-Ext1*t*	2.45	3.60	4.16	164.28	0.499	3.21	2.98
4	MCM-41-Ext2*t*	2.49	3.54	4.09	613.01	0.598	3.01	3.09
5	MCM-41-Ext3*t*	2.47	3.57	4.13	187.23	0.173	3.70	2.17
6	MCM-41-Ext4*t*	2.52	3.50	4.05	680.82	0.556	3.26	2.99
7	MCM-41-Co1*t*	2.35	3.76	4.34	23.62	0.089	2.41	1.76
8	MCM-41-Co2*t*	2.38	3.69	4.27	39.52	0.1092	1.22	1.78
9	MCM-41-Co3*t*	2.37	3.72	4.30	27.16	0.096	2.23	1.81
10	MCM-41-Co4*t*	2.41	3.68	4.25	46.68	0.1264	1.08	1.75
No.	**Nano-materials Silica source: Sodium silicate**	**2θ**	**d_{100} (nm)**	**a_o (nm)**	**S_{BET} (m^2/g)**	**Vp (cm^3/g)**	**Pore size W_{BJH} (nm)**	**Pore Size W_d (nm)**
1	As-synthesised MCM-41 s	2.33	3.79	4.37	17.10	0.049	1.13	1.36
2	MCM-41-Cal*s*	2.57	3.43	3.96	884.04	1.023	2.62	3.30
3	MCM-41-Ext1*s*	2.38	3.71	4.28	143.92	0.319	3.31	2.75
4	MCM-41-Ext2*s*	2.42	3.65	4.21	524.49	0.417	2.74	2.92
5	MCM-41-Ext3*s*	2.43	3.63	4.18	298.64	0.457	7.21	2.97
6	MCM-41-Ext4*s*	2.48	3.56	4.11	591.82	0.539	3.10	3.04
7	MCM-41-Co1*s*	2.26	3.91	4.51	15.949	0.082	5.95	1.84
8	MCM-41-Co2*s*	2.30	3.84	4.43	28.115	0.097	2.94	1.87
9	MCM-41-Co3*s*	2.32	3.81	4.39	26.668	0.090	1.49	1.79
10	MCM-41-Co4*s*	2.35	3.76	4.34	39.871	0.096	3.95	1.82
No.	**Nano-materials (Post-grafted)**	**2θ**	**d_{100} (nm)**	**a_o (nm)**	**S_{BET} (m^2/g)**	**Vp (cm^3/g)**	**Pore size W_{BJH} (nm)**	**Pore Size W_d (nm)**
1	MCM-41-Post-Cal*t*	2.58	3.42	3.95	43.78	0.079	6.51	1.52
2	MCM-41-Post-Ext2*t*	2.42	3.65	4.21	17.07	0.067	1.57	1.51
3	MCM-41-Post-Ext4*t*	2.49	3.55	4.09	19.64	0.050	2.07	1.49
4	MCM-41-Post-Cal*s*	2.60	3.39	3.92	29.04	0.207	2.90	2.19
5	MCM-41-Post-Ext2*s*	2.46	3.59	4.14	32.34	0.234	2.89	2.42
6	MCM-41-Post-Ext4*s*	2.51	3.52	4.06	42.76	0.242	2.27	2.40

d_{100} = Inter planar spacing, a_o = Unit cell dimension, S_{BET} = BET surface area, V_p = Pore volume, W_{BJH}, W_d = Pore size diameter (nm).

attached to the outer silica surfaces of post-grafted materials, which could block their mesopores and cause a decrease in their surface areas [27]. However, post-grafted amino functionalised materials synthesised from sodium silicate were observed to have slightly larger surface areas compared to their co-condensed counterparts.

Calcined nanomaterials Cal-MCM-41 *t* and Cal-MCM-41 *s* had the most significant specific surface areas and pore volumes with decreased pore diameters compared to the solvent-extracted nanomaterials. This could be due to the decomposition of the surfactant leading to the formation of more pores, structural shrinkage, and sintering of particles at a high calcination temperature [42].

For surfactant removal, the specific surface area and pore volume obtained showed that stirring the nanomaterials in an acid/alcohol medium for 15 min at room temperature led to the partial removal of surfactant from the mesopores. In contrast, more surfactant was removed after stirring for 6 h at 60℃, as seen in Table 2. The pore size diameter of the nanomaterials was evaluated using the Barrett-Joyner-Halenda (BJH) method and a geometrical model according to equation (1.1).

$$W_d = c.d_{100}\sqrt{(\frac{V_p}{1} + \rho V_p)} \quad (1.1)$$

Where "W_d" refers to the pore size, "c" is a constant dependent on the pore's geometry. For hexagonal models, it is equal to 1.155. "d_{100}" refers to the XRD inter-planar spacing (1 0 0), "V_p" denotes the mesoporous volume, while "ρ" is the pore wall density and is given as ca. 2.2 cm^3g^{-1} for siliceous materials [43]. The nanomaterials' BJH and geometrical pore size diameters were between ~ 1.05 to ~ 7.21 nm and ~ 1.36 to ~ 3.30 nm, respectively.

FTIR analysis of synthesised MSNs

FTIR was used to confirm the formation of a silica network and the presence of amino groups in the synthesised nanomaterials by evaluating their surface chemistry and verifying the removal of the surfactant from the mesopores. The FTIR spectra of solvent-extracted and amino co-condensed nanomaterials MCM-41-Ext2*t&s*, MCM-41-Ext4*t&s*, MCM-41-Co2*t&s*, and MCM-41-Co4*t&s* were compared with As-synthesised MCM-41 t&s and MCM-41-Cal*t&s* as seen in Fig. 3a and c. Fig. 3b and d show the FTIR spectra of amino post-grafted nanomaterials: MCM-41-Post-Cal*t&s*, MCM-41-Post-Ext2*t&s*, and MCM-41-Post-Ext4*t&s*. The IR spectra of all the nanomaterials revealed transmittance peaks between 3570–3200 cm^{-1} belonging to hydroxyl stretching vibrations from silanol groups and adsorbed water molecules with transmittance peaks between 1650–1590 cm^{-1} from deformed or twisted vibrations of absorbed water molecules δ(HOH).

Transmittance peaks from stretching vibrations of Si-O-Si (1130–1000 cm^{-1}) and Si-O (1000–900 cm^{-1}) with bending vibrations of Si-OH (950–810 cm^{-1}) belonging to silanol groups were also observed, indicating the formation of silica network [44] in all synthesised nanomaterials. However, shifts to a lower frequency for Si-OH bending vibrations were observed in all the post-grafted materials. The amino-functionalised nanomaterials also exhibited peaks that confirmed the formation of silica networks and modification with amino groups. Transmittance peaks (895–650 cm^{-1}) and (1650–1550 cm^{-1}) attributed to N-H bending δ(N-H) and NH_2 symmetric bending δ(NH_2) vibrations, respectively, were observed in all amino-functionalised nanomaterials confirming the covalent bonding of amino groups to the silica surfaces of the nanomaterials [45] and their retention after solvent extraction in the alcoholic medium at 60℃ for 6 h.

The transmittance peaks 2940–2915 cm^{-1} and 2870–2840 cm^{-1}, which were assigned to asymmetric stretching and symmetric stretching vibrations of methylene groups (CH_2), and the transmittance peaks 1470–1430 cm^{-1} from CH_2 bending vibrations of methylene groups, was due to alkyl ammonium vibrations of surfactant CTAB [46]. Compared with their as-synthesised nanomaterials, these peaks became weaker within the solvent-extracted and amino-functionalised (co-condensed and post-grafted) nanomaterials. This implied that parts of the CTAB

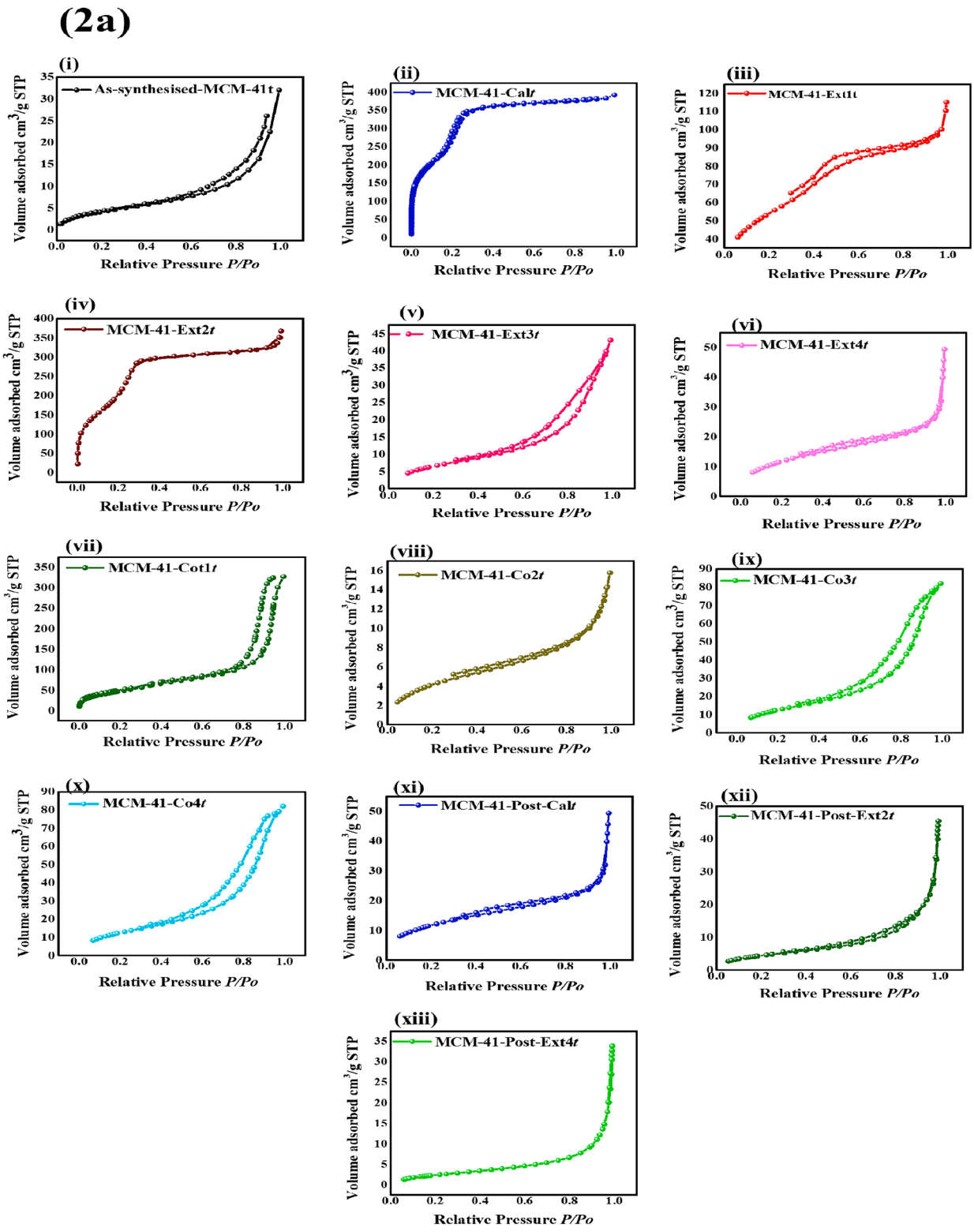

Fig. 2. (a): N_2 adsorption–desorption isotherms of MCM-41 nanomaterials synthesised using TEOS as silica source: (i) As-synthesised MCM-41*t*, (ii) MCM-41-Cal*t*, (iii) MCM-41-Ext1*t*, (iv) MCM-41-Ext2*t*, (v) MCM-41-Ext3*t*, (vi) MCM-41-Ext4*t*, (vii) MCM-41-Co1*t*, (viii) MCM-41-Co2*t*, (ix) MCM-41-Co3*t*, (x) MCM-41-Co4*t*, (xi) MCM-41-Post-Cal*t*, (xii) MCM-41-Post-Ext2*t*, (xiii) MCM-41-Post-Ext4*t*. The supporting dataset can be found at [36]. **(b):** N_2 adsorption-desorption isotherms of MCM-41 nanomaterials synthesised using Sodium silicate as silica source: (i) As-synthesised MCM-41*s*, (ii) MCM-41-Cal*s*, (iii) MCM-41-Ext1*s*, (iv) MCM-41-Ext2*s*, (v) MCM-41-Ext3*s*, (vi) MCM-41-Ext4*s*, (vii) MCM-41-Co1*s*, (viii) MCM-41-Co2*s*, (ix) MCM-41-Co3*s*, (x) MCM-41-Co4*s*, (xi) MCM-41-Post-Cal*s*, (xii) MCM-41-Post-Ext2*s*, (xiii) MCM-41-Post-Ext4*s*. The supporting dataset can be found at [36]

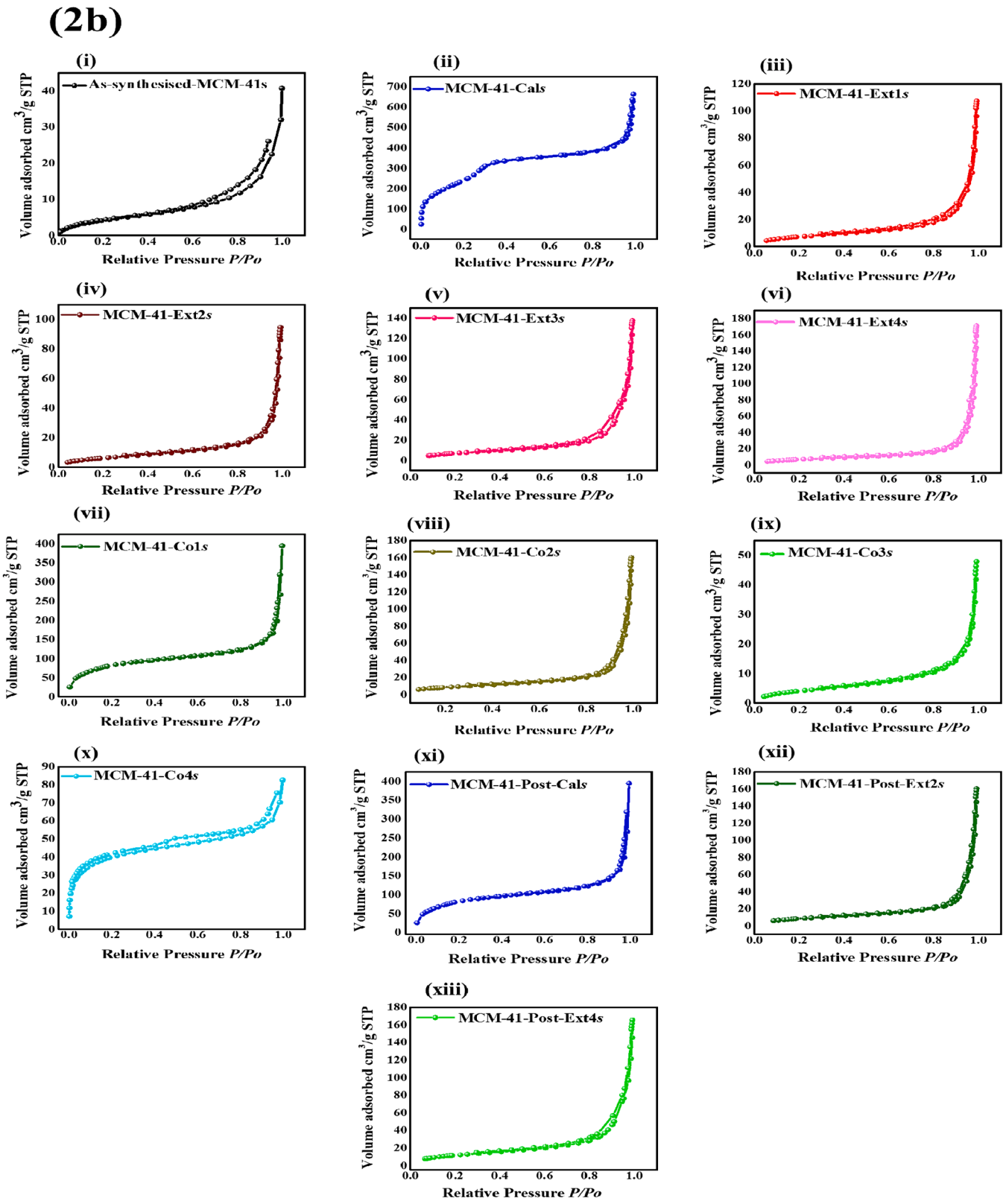

Fig. 2. (*continued*).

molecules had been removed from the nanomaterials. These peaks were not seen in the calcined materials due to the complete surfactant removal by calcination.

Thermogravimetric analysis of synthesised MSNs

Thermogravimetric analysis (TGA) was used to evaluate the number of organic moieties attached to the amino-functionalised nanomaterials and quantify the amount of surfactant removed from the nanomaterials.

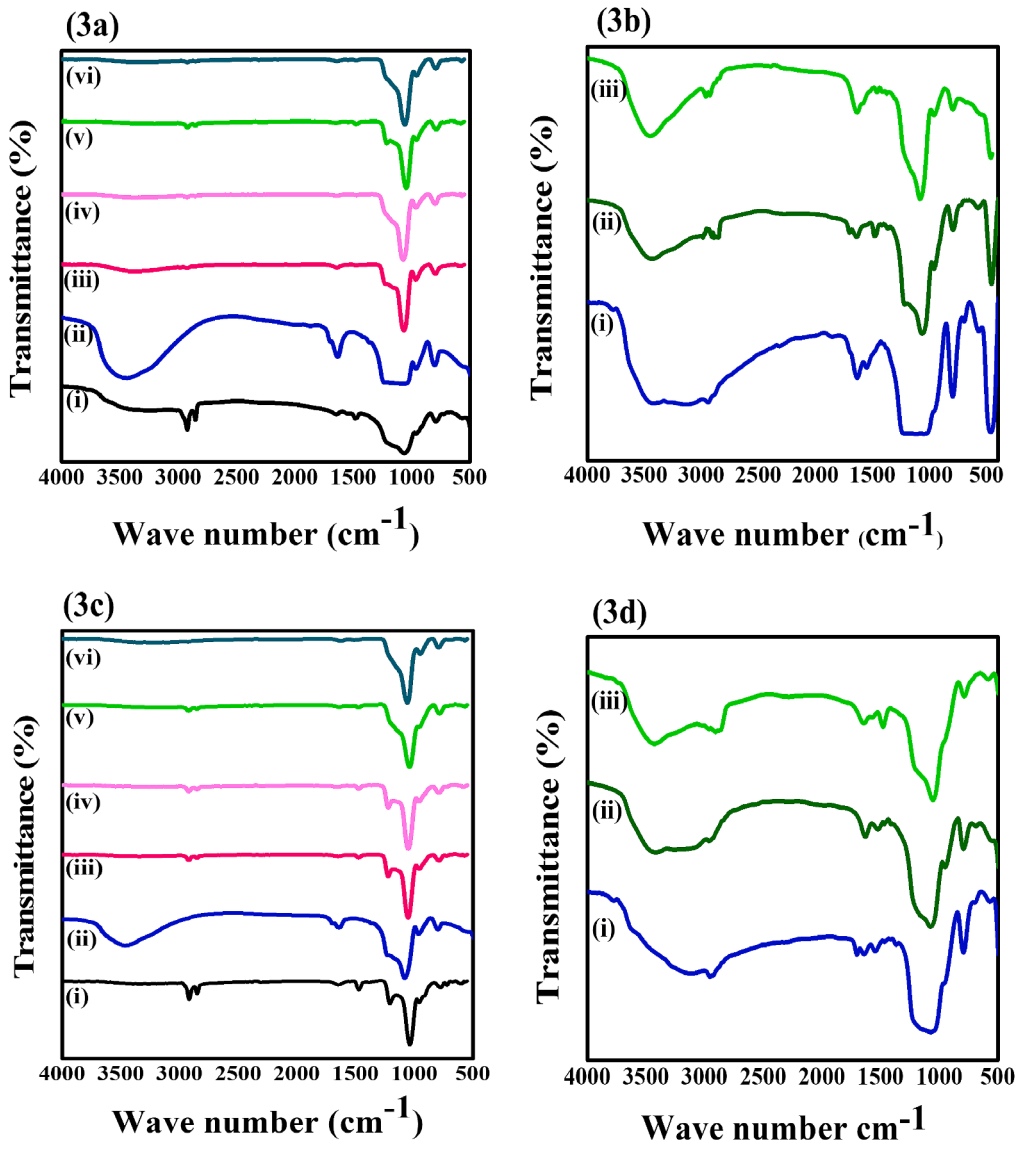

Fig. 3. (a): FTIR Spectra of MCM-41 nanomaterials synthesised using TEOS as silica source: (i) As-synthesised MCM-41*t*, (ii) MCM-41-Cal*t*, (iii) MCM-41-Ext2*t*, (iv) MCM-41-Ext4*t*, (v) MCM-41-Co2*t*, (vi) MCM-41-Co4*t*. **(b):** FTIR Spectra of post-grafted MCM-41 nanomaterials with TEOS as silica source: (i) MCM-41-Post-Cal*t*, (ii) MCM-41-Post-Ext2*t*, (iii) MCM-41-Post-Ext4*t*. **(c):** FTIR Spectra of MCM-41 nanomaterials synthesised using Sodium Silicate as silica source: (i) As-synthesised MCM-41*s*, (ii) MCM-41-Cal*s*, (iii) MCM-41-Ext2*s*, (iv) MCM-41-Ext4*s*, (v) MCM-41-Co2*s*, (vi) MCM-41-Co4*s*. **(d):** FTIR Spectra of post-grafted MCM-41 nanomaterials with Sodium Silicate as silica source: (i) MCM-41-Post-Cal*s*, (ii) MCM-41-Post-Ext2*s*, (iii) MCM-41-Post-Ext4*s*. The supporting dataset can be found at [36]

The percentage weight loss for the nanomaterials was estimated within the range of 25℃ to 800℃, and the TGA curves were represented in Fig. 4a–d. The TGA curves of the calcined and solvent-extracted nanomaterials showed that weight loss occurred at three different temperature regions. The initial weight loss was between 25℃ and 150℃ due to the thermo-desorption/drying of absorbed water molecules from the nanomaterials. The second weight loss was between 150℃ and 450℃ due to the decomposition of the surfactant, and the third between 450℃ and 800℃ due to the condensation of Si-OH to Si-O-Si [47].

The amount of surfactant in the as-synthesised and calcined nanomaterials was calculated to be 34.27 %, 1.023 %, 50.07 %, and 1.58 % for as-synthesized-MCM-41 *t*, MCM-41-call, as-synthesized-MCM-41 s, and MCM-41-calls, respectively. Solvent-extracted materials had weight losses of 4.20 %, 6.01 %, 5.21 %, and 9.71 % for MCM-41-Ext2*t*, MCM-41-Ext4*t*, MCM-41-Ext2*s* and MCM-41-Ext4*s*, respectively. The data showed that most of the CTAB molecules had been removed from nanomaterials, and surfactant removal using methanol as solvent had a higher surfactant removal efficiency than ethanol.

For amino-functionalised nanomaterials, the weight loss observed between 300 and 600℃ can be attributed to the decomposition of amine groups from their mesopores [28,48]. MCM-41-Co2*t*, MCM-41-Co4*t*, MCM-41-Co2*s*, and MCM-41-Co4*s* had 10.69 %, 9.1 %, 14.71 %, and 12.96 % amino groups, respectively. In post-grafted nanomaterials, MCM-41-Post-Cal1*t*, MCM-41-Post-Ext2*t*, and MCM-41-Post-Ext4*t* had 8.26 %, 10.07 % and 9.63 % amino groups, respectively, while MCM-41-Post-Cal*s*, MCM-41-Post-Ext2*s*, and MCM-41-Post-Ext4*s* had 6.76 %, 13.60 %, and 10.13 % amino groups, respectively.

SEM of synthesised MSNs

The effect of surfactant removal and surface functionalisation on the choice of silica source used during synthesis was seen to have some impact on the morphology of the synthesised materials. SEM images of non-functionalized and co-condensed amino functionalised

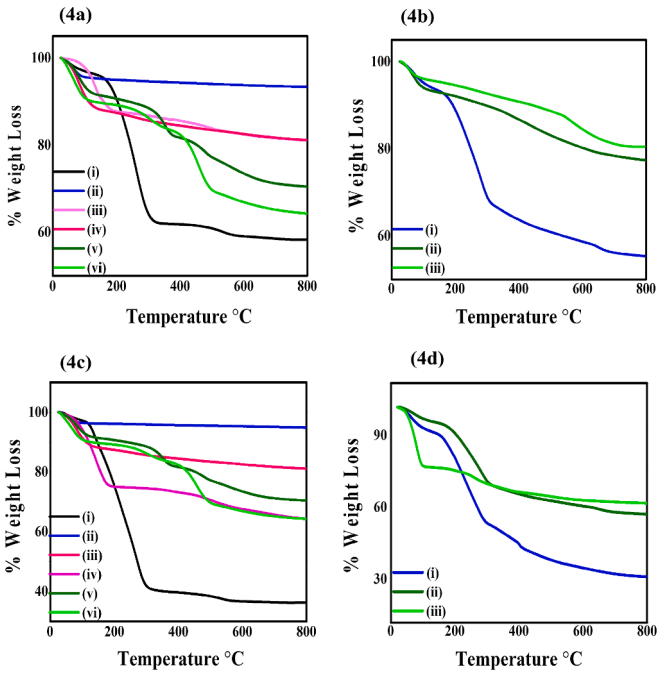

Fig. 4. (a): TGA curves of MCM-41 nanomaterials synthesised using TEOS as silica .
source: (i) As-synthesised MCM-41*t*, (ii) MCM-41-Cal*t*, (iii) MCM-41-Ext2*t*, (iv) MCM-41-Ext4*t*, (v) MCM-41-Co2*t*, (vi) MCM-41-Co4*t*. **(b):** TGA curves of post-grafted MCM-41 nanomaterials with TEOS as silica source: (i) MCM-41-Post-Cal*t*, (ii) MCM-41-Post-Ext2*t*, (iii) MCM-41-Post-Ext4*t*. **(c):** TGA curves of MCM-41 nanomaterials synthesised using Sodium Silicate as silica source: (i) As-synthesised MCM-41*s*, (ii) MCM-41-Cal*s*, (iii) MCM-41-Ext2*s*, (iv) MCM-41-Ext4*s*, (v) MCM-41-Co2*s*, (vi) MCM-41-Co4*s*. **(d):** TGA curves of post-grafted MCM-41 nanomaterials with Sodium Silicate as silica source: (i) MCM-41-Post-Cal*s*, (ii) MCM-41-Post-Ext2*s*, (iii) MCM-41-Post-Ext4*s*. The supporting dataset can be found at [36]

nanomaterials synthesised with tetraethyl orthosilicate are presented in Fig. 5a–g. Spherical-shaped particles with smooth surfaces were observed in As-synthesized-MCM-41*t* (Fig. 5a), which was preserved after calcination. The spherical-shaped nanoparticles MCM-41-Cal*t* (Fig. 5b) obtained after calcination suggest that a high rate of silica condensation occurred during their synthesis, leading to their spherical formation [1,2]. Spherical-shaped nanoparticles MCM-41-Ext4*t* (Fig. 5d) with larger particle sizes were observed after as-synthesized-MCM-41*t* was treated in HCl/MeOH. This could be attributed to less structural shrinkage from solvent extraction at a lower temperature than calcination, requiring a higher temperature. Also, the aggregation of smaller particles to form larger particles is thermodynamically enhanced at lower temperatures [49]. In contrast, well-dispersed rod-like nanoparticles MCM-41-Ext2*t* (Fig. 5c) were observed after treatment in HCl/EtOH solvent, which could result from the choice of solvent, stirring time, or intensity used during solvent extraction. During synthesis, alcohols have been reported to affect the structural morphology of hollow spherical-shaped MCM-41 nanomaterials [50]. At the same time, those with long chains have also been reported to create new morphological phases from existing ones. For instance, hexanol was used to transit MCM-41 from a hexagonal to a lamellar phase by Argen et al. [52,51]. However, Boukoussa et al. reported a change in the morphology of Si-MCM-41 from elongated agglomerates to rod-like nanoparticles after solvent extraction in HCl/EtOH solvent for 2 h at 60C [52].

For amino-functionalised nanomaterials (Fig. 5e–g), an agglomerate of spherical-shaped nanoparticles with non-uniform size distribution was observed before solvent extraction (MCM-41-Co*t*). This could be attributed to fluctuations in the dropping rate of TEOS or APTES during synthesis, which causes uneven silica precipitation [53]. After solvent extraction, the spherical-shaped nanoparticles were retained with less agglomeration, as seen in Fig. 5e and Fig. 5f, suggesting that the alcohols used for solvent extraction reduced particle agglomeration [54].

The SEM images of non-functionalized and co-condensed amino functionalised nanomaterials synthesised with sodium silicate are presented in Fig. 6a–g. It was observed that as-synthesised-MCM-41*s* (Fig. 6a) had a sheet-like structure, which broke down after calcination to form an agglomerate of tiny spherical particles MCM-41-Cal*s* (Fig. 6b). This indicates that the particles were formed by the aggregation of very fine nano-sized particles. Solvent-extracted nanomaterials MCM-41-Ext2*s* had wire-like particles (Fig. 6c). At the same time, MCM-41-Ext4s formed an aggregate of sponge-like particles (Fig. 6d). The amino-functionalised nanomaterials (Fig. 6e–g) before (MCM-41-Co*s*) and after solvent extraction retained their aggregate of spherical shapes.

The SEM images of the post-grafted nanomaterials are shown in Fig. 7a–f. Post-grafted nanomaterials MCM-41-Post-Cal*t*, MCM-41-Post-Ext2*t*, and MCM-41-Post-Ext4*t* (Fig. 7a–c) retained their spherical and rod-like shapes before and after post-grafting while an aggregate of nanomaterials was observed in post grafted MCM-41-Post-Cal*s*, MCM-41-Post-Ext2*s* and MCM-41-Post-Ext4*s* (Fig. 7d–f).

TEM of synthesised MSNs

The TEM images of the calcined nanomaterials MCM-41-Cal*t*, MCM-41-Post-Cal*t*, MCM-41-Cal*s*, and MCM-41-Post-Cal*s* (Fig. 8a–d), respectively, were obtained to determine the porosity of the nanomaterials. The calcined nanomaterials revealed dark and white spots representing the pore system of the nano-materials. The dark spots could be attributed to the presence of oxygen and silica atoms on the walls of the nanomaterials, and the white spots might indicate the presence of mesopores [55]. MCM-41-Cal*s* (Fig. 8c) revealed long strips, indicating that the mesoporous material had long-range channels [56] and was more orderly compared to MCM-41-Cal*t* (Fig. 8a). After amino functionalisation, there were changes in the structure ordering and pore structure of the functionalised nanomaterials. MCM-41-Post-Cal*t* (Fig. 8b) and MCM-41-Post-Cal*s* (Fig. 8d) had less prominent pore structures with smooth surfaces compared to their parent nanomaterials MCM-41-Cal*t* (Fig. 8a) and MCM-41-Cal*s* (Fig. 8c). This was similar to a report by Du et al., 2019 [57], where post-grafted amino functionalised nanomaterials were synthesised using TEOS as a silica source. Less structural ordering was also observed in MCM-41-Post-Cal*s* as the long strips indicating long-range channels seen in MCM-41-Cal*s* were absent.

Conclusion

The study demonstrated that various non-functionalised and amino-functionalised nanomaterials with different physicochemical and textural properties can be synthesised using different silica sources, surfactant removal methods, and surface functionalisation schemes. MCM-41 nanomaterials were synthesised using tetra ethyl orthosilicate and sodium silicate as silica sources and surface functionalised with amino groups employing co-condensation and post-grafting methods. MCM-41 nanomaterials synthesised with sodium silicate were observed to have less mesoporous ordering compared to their TEOS counterparts. Also, co-condensed amino functionalised nanomaterials produced less orderly mesoporous structures from both silica sources than their post-grafted counterparts. The effect of surfactant removal methods, calcination, and acid solvent extraction methods on the physicochemical and textural properties of non-functionalised and amino-functionalised nanomaterials was evaluated. An increase in the 2θ values of non-functionalised nanomaterials with a decrease in their d-spacing and unit-cell parameters was observed.

In contrast, a decrease in the 2θ values and increased d-spacing and unit-cell parameters were noticed in amino-functionalised nanomaterials synthesised from both silica sources. After solvent extraction, BET and FTIR studies confirmed that amino groups were retained within

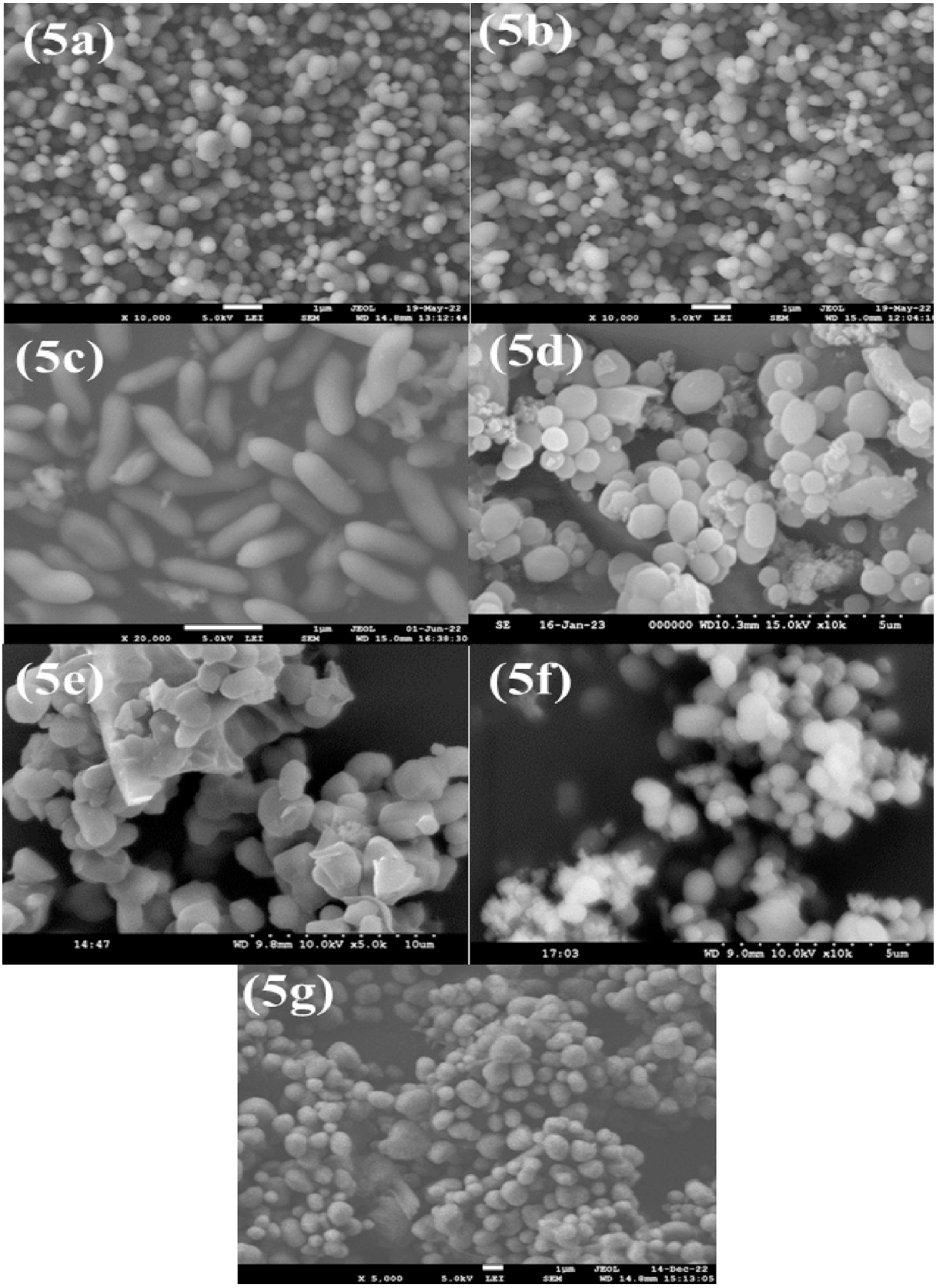

Fig. 5. SEM images of MCM-41 nanomaterials synthesised using TEOS as silica source: (a) As-synthesised MCM-41*t*, (b) MCM-41-Cal*t*, (c) MCM-41-Ext2*t*, (d) MCM-41-Ext4*t*, (e) MCM-41-Co*t*, (f) MCM-41-Co2*t*, (g) MCM-41-Co4*t*

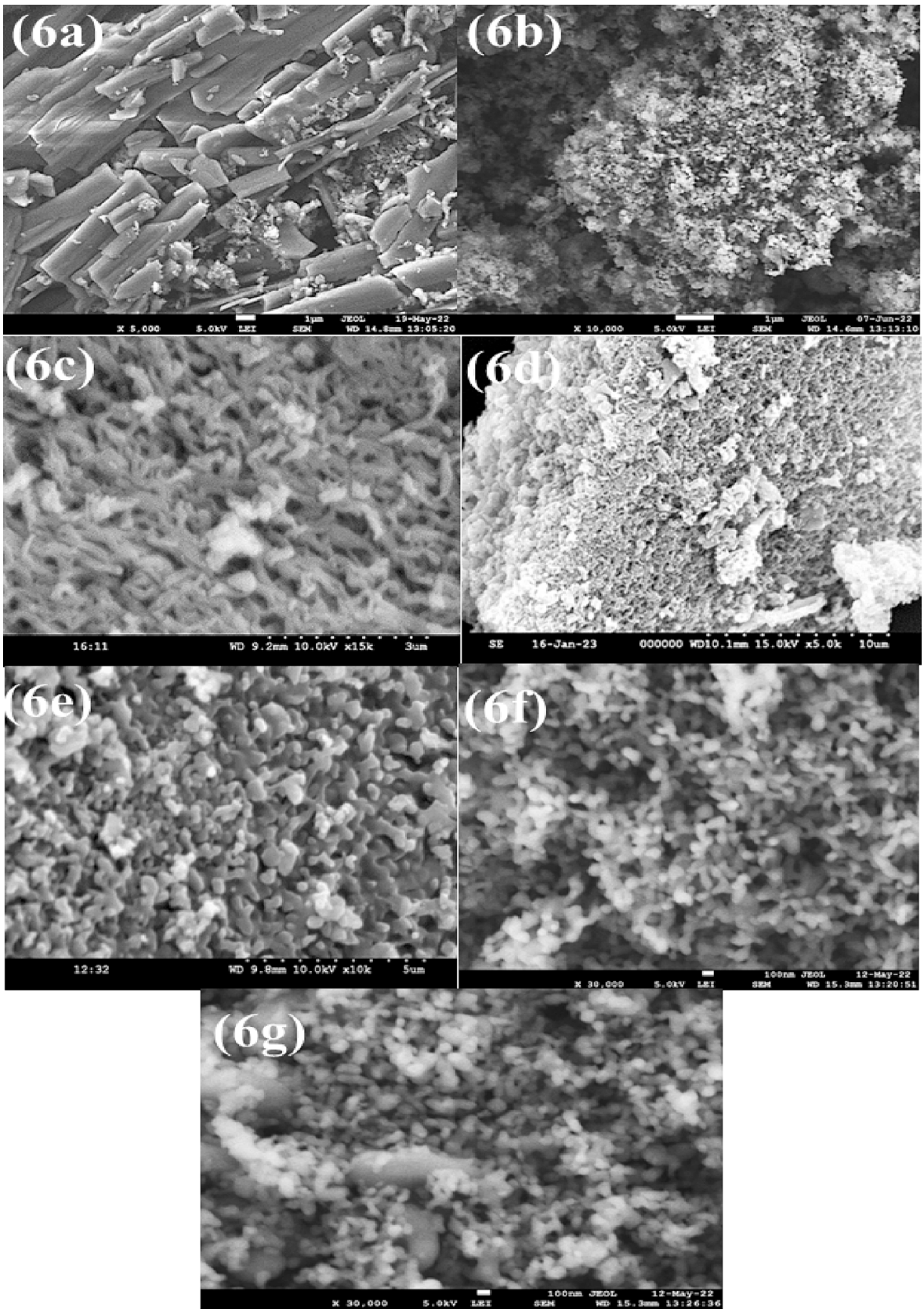

Fig. 6. SEM images of MCM-41 nanomaterials synthesised using sodium silicate as silica .
source: (a) As-synthesised MCM-41*s*, (b) MCM-41-Cal*s*, (c) MCM-41-Ext2*s*, (d) MCM-41-Ext4*s*, (e) MCM-41-Co*s*, (f) MCM-41-Co2*s*, (g) MCM-41-Co4*s*

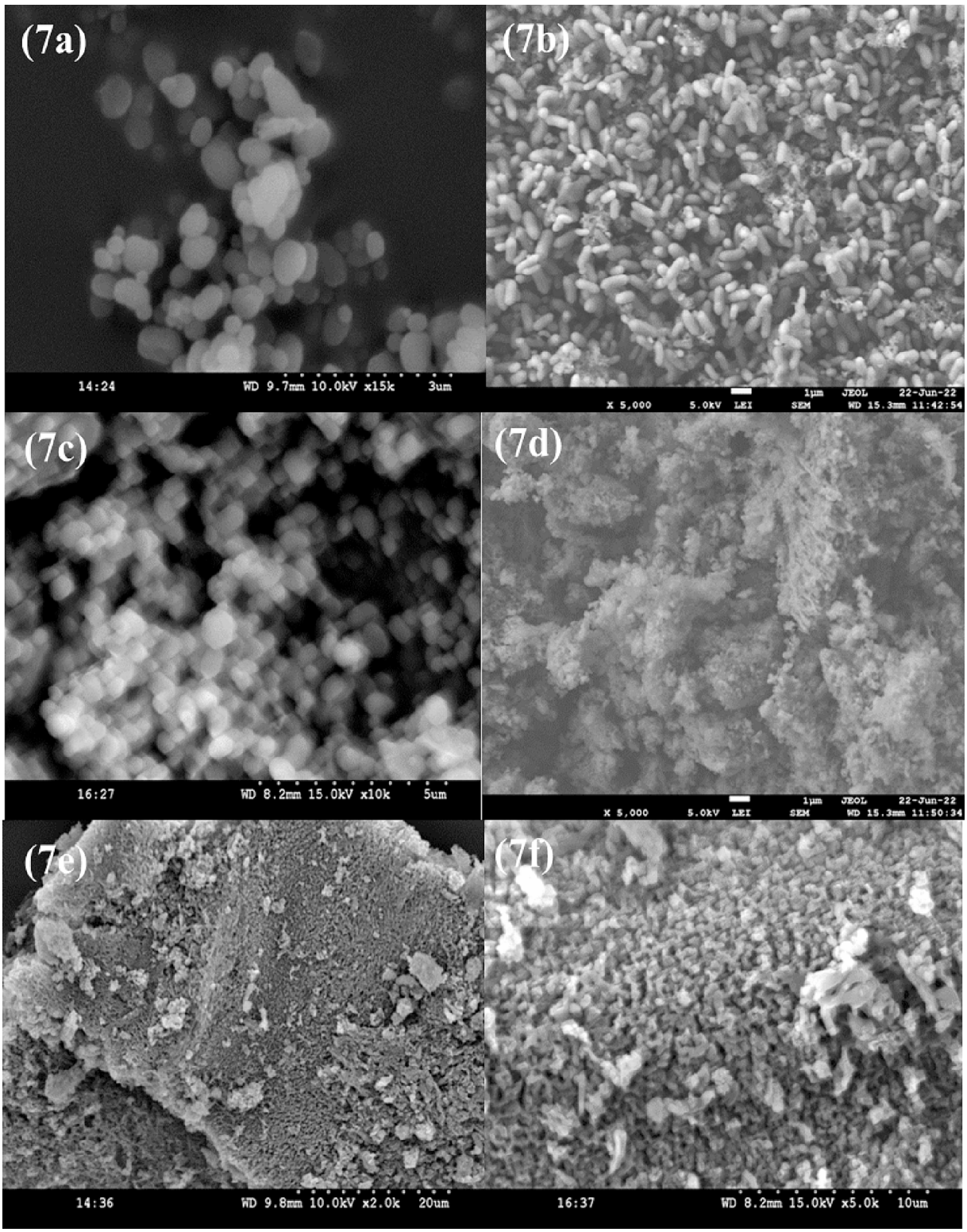

Fig. 7. SEM images of MCM-41 nanomaterials synthesised using TEOS and Sodium silicate as silica source: (a) MCM-41-Post-Cal*t*, (b) MCM-41-Post-Ext2*t*, (c) MCM-41-Post-Ext4*t*, (d) MCM-41-Post-Cal*s*, (e) MCM-41-Post-Ext2*s*, (f) MCM-41-Post-Ext4*s*

the silica frameworks. TGA analysis showed that methanol was a better solvent for removing surfactant from the solvent-extracted nanomaterials. The SEM images of the synthesised nanomaterials revealed various particle morphologies that can be used for different scientific applications. Also, the morphologies of the amino functionalised nanomaterials synthesised from both silica sources were not affected by solvent extraction and the surface functionalisation method employed.

CRediT authorship contribution statement

Josephine Oluwagbemisola Tella: Writing – original draft, Methodology, Investigation, Funding acquisition, Formal analysis, Data

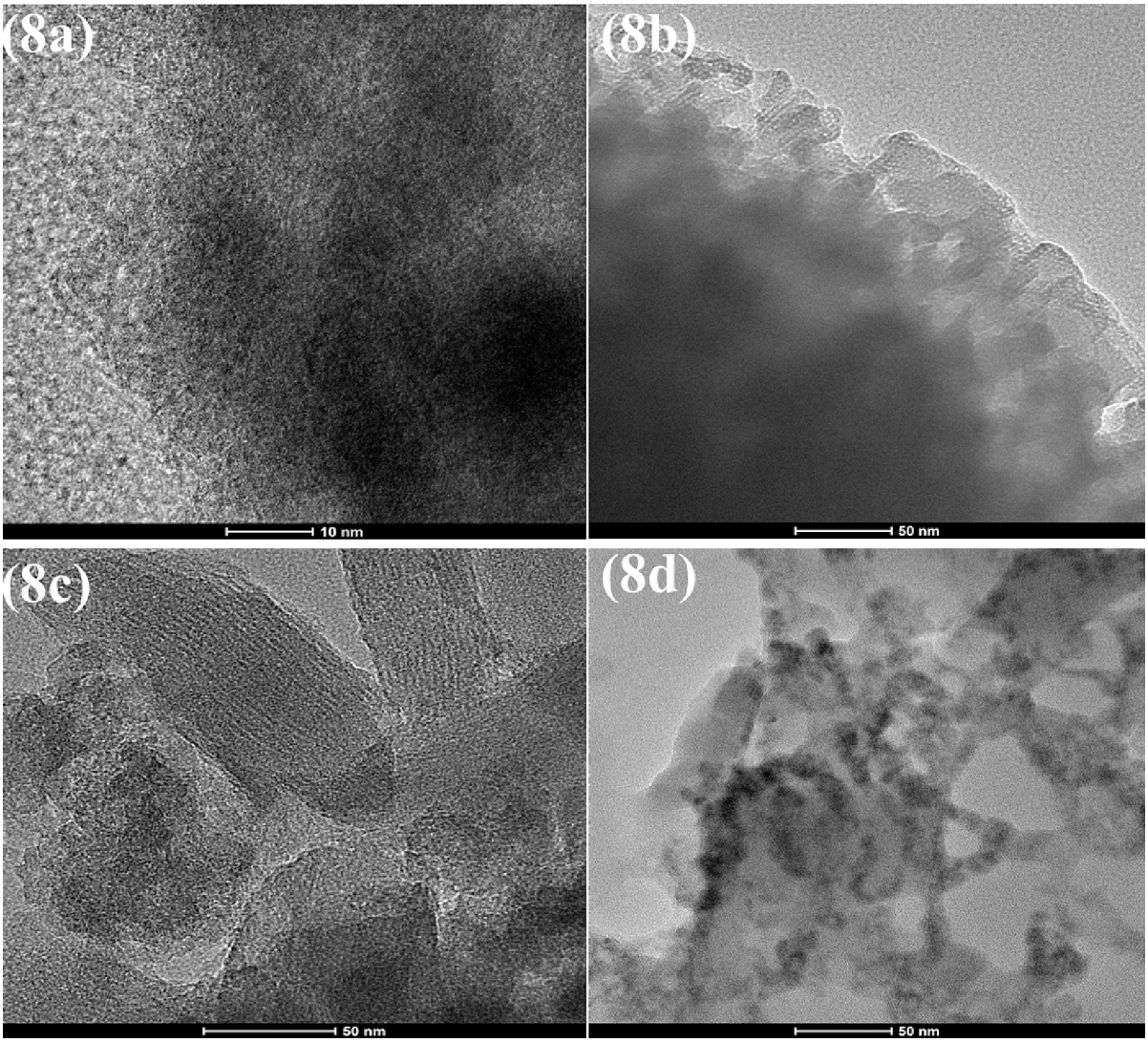

Fig. 8. TEM images of the calcined nanomaterials: (a) MCM-41-Cal*t*, (b) MCM-41-Post-Cal*t*, (c) MCM-41-Cal*s*, (d) MCM-41-Post-Cal*s*.

curation. **Kolawole Oluseyi Ajanaku:** Writing – review & editing, Supervision, Project administration. **Joseph Adeyemi Adekoya:** Writing – review & editing, Supervision, Project administration, Methodology, Conceptualization. **Rajkumar Banerjee:** Supervision, Resources, Project administration, Formal analysis. **Chitta Ranjan Patra:** Resources, Project administration, Funding acquisition, Formal analysis. **Srinivas Pavuluri:** Resources, Project administration, Data curation. **Bojja Sreedhar:** Validation, Resources, Project administration, Data curation.

Declaration of competing interest

The authors declare that they have no known competing financial interests or personal relationships that could have appeared to influence the work reported in this paper.

Acknowledgements

Tella, Josephine Oluwagbemisola is grateful to CSIR-TWAS Italy and CSIR-Indian Institute of Chemical Technology (CSIR-IICT), Hyderabad, India, for the Sandwich Post Graduate Fellowship award (FR: 3240316975) under the supervision of Prof. Rajkumar Banerjee and Prof. Chittaranjan Patra of Applied Biology Division. The authors are also grateful to Covenant University Centre for Research, Innovation, and Discovery (CUCRID) for the financial support to publish this article.

References

[1] C.T. Kresge, M.E. Leonowicz, W.J. Roth, J.C. Vartuti, J.S. Beek, Ordered mesoporous molecular sieves synthesised by a liquid-crystal template mechanism, Nature 359 (1992) 710–712, https://doi.org/10.1038/359710a0.

[2] J. S. Beck, J. C. Vartuli W. J. Roth, M. E. Leonowicz, C. T, Kresge, K. D. Schmitt, CT-W Chu, D. H. Olson, E. W, Sheppard, S.B. McCullen, J. B. Higgins, J. L. Schlenker, A new family of mesoporous molecular sieves prepared with liquid crystal templates, J. Am. Chem. Soc. 114 (27) (1992) 10834-10843. https://doi.org/10.1021/ja00053a020.

[3] A. Maleki, M. Hamidi, Dissolution enhancement of a model poorly water-soluble drug, atorvastatin, with ordered mesoporous silica: comparison of MSF with SBA-15 as drug carriers, Expert Opin. Drug Deliv. 13 (2) (2016) 171–181, https://doi.org/10.1517/17425247.2015.1111335.

[4] G.V. Deodhar, M.L. Adams, B.G. Trewyn, Controlled release and intracellular protein delivery from mesoporous silica nanoparticles, Biotechnol. J. 12 (1) (2017) 1600408, https://doi.org/10.1002/biot.201600408.

[5] A. Llopis-lorente, B. Lozano-torres, A. Bernardos, R. Martínez-máñez, F. Sancenón, Mesoporous silica materials for controlled delivery based on enzymes, J. Mater. Chem. 5 (17) (2017) 3069–3083, https://doi.org/10.1039/C7TB00348J.

[6] J. Wen, K. Yang, F. Liu, H. Li, Y. Xu, S. Sun, Diverse gatekeepers for mesoporous silica nanoparticle-based drug delivery systems, Chem. Soc. Rev. 46 (19) (2017) 6024–6045, https://doi.org/10.1039/C7CS00219J.

[7] J.O. Tella, J.A. Adekoya, K.O. Ajanaku, Mesoporous silica nanocarriers as drug delivery systems for anti-tubercular agents: a review, R. Soc. Open Sci. 9 (2022) 220013, https://doi.org/10.1098/rsos.220013.

[8] L.P. Singh, S.K. Bhattacharyya, R. Kumar, G. Mishra, U. Sharma, G. Singh, S. Ahalawat, Sol-Gel processing of silica nanoparticles and their applications, Adv. Colloid Interface Sci. 214 (1) (2014) 17–37, https://doi.org/10.1016/j.cis.2014.10.007.

[9] H. Setyawan, R. Balgis, Mesoporous silicas prepared from sodium silicate using gelatin templating, Asia Pac. J. Chem. Eng. 7 (3) (2012) 448–454, https://doi.org/10.1002/apj.593.

[10] Y.-S. Kang, H.I. Lee, Y. Zhang, Y.J. Han, J.E. Yie, G.D. Stucky, J.M. Kim, Direct synthesis of ordered mesoporous materials constructed with polymer-silica hybrid frameworks, Chem. Commun. (2004) 1524–1525, https://doi.org/10.1039/B402037E.

[11] S. Jabariyan, M.A. Zanjanchi, A simple and fast sonication procedure to remove surfactant templates from mesoporous MCM-41, Ultrason. Sonochem. 19 (5) (2012) 1087–1093, https://doi.org/10.1016/j.ultsonch.2012.01.012.

[12] T.T.H. Thi, V.D. Cao, T.N.Q. Nguyen, D.T. Hoang, V.C. Ngo, D.H. Nguyen, Functionalized mesoporous silica nanoparticles and biomedical applications, Mater. Sci. Eng. C 99 (2019) 631–656, https://doi.org/10.1016/j.msec.2019.01.129.

[13] Z. Li, J.C. Barnes, A. Bosoy, J.F. Stoddart, J.I. Zink, Mesoporous silica nanoparticles in biomedical applications, Chem. Soc. Rev. 41 (2012) 2590–2605, https://doi.org/10.1039/C1CS15246G.

[14] H. Shibata, T. Ogura, T. Mukai, T. Ohkubo, H. Sakai, M. Abe, Direct synthesis of mesoporous titania particles having a crystalline wall, J. Am. Chem. Soc. 127 (2005) 16396–16397, https://doi.org/10.1021/ja0552601.

[15] I.R. Fernando, D.P. Ferris, M. Frasconi, D. Malin, E. Strekalova, M.D. Yilmaz, M. W. Ambrogio, M.M. Algaradah, M.P. Hong, X. Chen, M.S. Nassar, Y.Y. Botros, V. L. Cryns, J.F. Stoddart, Esterase- and pH-responsive poly(β-amino ester)-capped mesoporous silica nanoparticles for drug delivery, Nanoscale 7 (16) (2015) 7178–7183, https://doi.org/10.1039/C4NR07443B.

[16] L.C. Mugica, B. Rodríguez-Molina, S. Ramos, A. Kozina, Surface functionalization of silica particles for their efficient fluorescence and stereo selective modification, Colloids Surf. A Physicochem. Eng. Asp. 500 (2016) 79–87, https://doi.org/10.1016/j.colsurfa.2016.04.002.

[17] Y. Nakahara, T. Takeuchi, S. Yokoyama, K. Kimura, Quantitative ^{1}H NMR analysis of reacted silanol groups in silica nanoparticles chemically modified with monochlorosilanes, Surf. Interface Anal. 43 (2011) 809–815, https://doi.org/10.1002/sia.3633.

[18] S. Daniel, G. Mariappan, S. Chinnathambi, S. Kannan, Co-solvent and local environment effects of vanadium incorporation on MCM-41 catalysts for selective oxidation reactions, ACS Appl. Nano Mater. 5 (1) (2022) 288–302, https://doi.org/10.1021/acsanm.1c02960.

[19] A. Stavitskaya, A. Glotov, F. Pouresmaeil, K. Potapenko, E. Sitmukhanova, K. Mazurova, E. Ivanov, E.A. Kozlova, V.A. Vinokurov, Y. Lvov, CdS quantum dots in hierarchical mesoporous silica templated on clay nanotubes: implications for photocatalytic hydrogen production, ACS Appl. Nano Mater. 5 (1) (2022) 605–614, https://doi.org/10.3390/pharmaceutics14071309.

[20] M. Varache, I. Bezverkhyy, F. Bouyer, R. Chassagnon, F. Baras, F. Bouyer, Improving structural stability of water-dispersed MCM-41 silica nanoparticles through post-synthesis pH aging process, J. Nanopart. Res. 17 (9) (2015) 356, https://doi.org/10.1007/s11051-015-3147-6.

[21] M. Davidson, Y. Ji, G.J. Leong, N.C. Kovach, B.G. Trewyn, R.M. Richards, Hybrid mesoporous silica/noble-metal nanoparticle materials-synthesis and catalytic applications, ACS Appl. Nano Mater. 1 (9) (2018) 4386–4400, https://doi.org/10.1021/ACSANM.8B00967.

[22] A. Ulu, S.A.A. Noma, S. Koytepe, B. Ates, Chloro-modified magnetic Fe_3O_4@MCM-41 core-shell nanoparticles for L-Asparaginase immobilization with improved catalytic activity, reusability, and storage stability, Appl. Biochem. Biotechnol. 187 (3) (2019) 938–956, https://doi.org/10.1007/s12010-018-2853-9.

[23] S. Huh, J.Y. Wiench, M. Pruski, S.-Y. Lin, Organic Functionalization and morphology control of mesoporous silicas via a co-condensation synthesis method, Chem. Mater. 15 (2003) 4247–4256, https://doi.org/10.1021/cm0210041.

[24] T.R. Pauly, V. Petkov, Y. Liu, S.J.L. Billinge, T. Pinnavaia, Role of framework sodium versus local framework structure in determining the hydrothermal stability of MCM-41 mesostructures, J. Am. Chem. Soc. 124 (1) (2002) 97–103, https://doi.org/10.1021/ja0118183.

[25] K.M. Parida, D. Rath, Amine functionalized MCM-41: An active and reusable catalyst for Knoevenagel condensation reaction, J. Mol. Catal. A Chem. 310 (2009) 93–100, https://doi.org/10.1016/j.molcata.2009.06.001.

[26] P. Fu, T. Yang, J. Feng, H. Yang, Synthesis of mesoporous silica MCM-41 using sodium silicate derived from copper ore tailings with an alkaline molted-salt method, J. Ind. Eng. Chem. 29 (2015) 338–343, https://doi.org/10.1016/j.jiec.2015.04.012.

[27] L. Mercier, T.J. Pinnavaia, Heavy metal ion adsorbents formed by the grafting of a thiol functionality to mesoporous silica molecular sieves: factors affecting Hg(II) uptake, Environ. Sci. Technol. 32 (1998) 2749–2754, https://doi.org/10.1021/es970622t.

[28] F. Twaiq, M.S. Nasser, S.A. Onaizi, Effect of the degree of template removal from mesoporous silicate materials on their adsorption of heavy oil from aqueous solution, Front. Chem. Sci. Eng 8 (2014) 488–497, https://doi.org/10.1007/s11705-014-1459-1.

[29] J. Wei, L.K. Zou, Synthesis of magnetical microspheres with tunable large pore mesostructures, J. Porous. Mater. 23 (2016) 577–581, https://doi.org/10.1007/s10934-015-0112-9.

[30] R. Schmidt, D. Akporiayea, M. Stöcker, O.H. Ellestad, Synthesis of Al-Containing MCM-41 Materials: Template Interaction and Removal, in: J. Weitkamp, H. G. Karge, H. Pfeifer, W. Hölderich (Eds.), Studies in Surface Science and Catalysis, vol. 84, Elsevier, 1994, pp. 61–68, https://doi.org/10.1016/S0167-2991(08)64097-5.

[31] B.B. Ma, L.Z. Zhuang, S.X. Chen, Rapid synthesis of tunable-structured short-pore SBA-15 and its application on CO_2 capture, J. Porous Mater. 23 (2016) 529–537, https://doi.org/10.1007/s10934-015-0106-7.

[32] O. Ajumobi, B. Wang, A. Farinmade, J. He, J.A. Valla, V.T. John, Design of nanostraws in amine-functionalized MCM-41 for improved adsorption capacity in carbon capture, Energ. Fuel 37 (16) (2023) 12079–12088, https://doi.org/10.1021/acs.energyfuels.3c01318.

[33] W. Klinthong, K.-J. Chao, C.-S. Tan, CO_2 capture by As-synthesized amine functionalized MCM-41 prepared through direct synthesis under basic condition, Ind. Eng. Chem. Res. 52 (29) (2013) 9834–9842, https://doi.org/10.1021/ie400865n.

[34] K. Yoncheva, M. Popova, A. Szegedi, J. Mihaly, B. Tzankov, N. Lambov, S. Konstantinov, V. Tzankova, F. Pessina, M. Valoti, Functionalized mesoporous silica nanoparticles for oral delivery of budesonide, J. Solid State Chem. 211 (2014) 154–161, https://doi.org/10.1016/j.jssc.2013.12.020.

[35] Y. Ma, H. Chen, Y.C. Shi, S.L. Yuan, Low cost synthesis of mesoporous molecular sieve MCM-41 from wheat straw ash using CTAB as surfactant, Mater. Res. Bull. 77 (2016) 258–264, https://doi.org/10.1016/j.materresbull.2016.01.052.

[36] J. Tella, K. Ajanaku, J. Adekoya, R. Banerjee, C. Patra, P. Srinivasu, B. Sreedhar, "Physicochemical and textural properties of amino-functionalised mesoporous silica nanomaterials from different silica sources", Mendeley Data, V2, 2023. https://doi.org/10.17632/fmy76wpjdm.2.

[37] M. Thommes, K. Kaneko, A.V. Neimark, J.P. Oliver, F. Rodriguez-Reinoso, J. Rouquerol, K.S.W. Sing, Physisorption of gases, with special reference to the evaluation of surface area and pore size distribution (IUPAC Technical Report), Pure Appl. Chem. 38 (1) (2015) 1051–1069, https://doi.org/10.1515/pac-2014-1117.

[38] S. Kaiprommarat, S. Kongparakul, P. Reubroycharoen, G. Guan, C. Samart, Highly efficient sulfonic MCM-41 catalyst for furfural production: furan-based biofuel agent, Fuel 174 (2016) 189–196, https://doi.org/10.1016/j.fuel.2016.02.011.

[39] F. Adam, C.W. Kueh, Phenyl-amino sulfonic solid acid-MCM-41 complex: a highly active and selective catalyst for synthesising mono-alkylated products in the solvent free tert-butylation of phenol, J. Taiwan Inst. Chem. Eng. 45 (2014) 713–723, https://doi.org/10.1016/j.jtice.2013.07.008.

[40] M. Masteri-Farahani, M. Modarres, Superiority of activated carbon versus MCM-41 for the immobilization of molybdenum dithiocarbamate complex as heterogeneous epoxidation catalyst, Chemistry 2 (2017) 1163–1169, https://doi.org/10.1002/slct.201601781.

[41] M. Colilla, M. Vallet-Regí, Ordered mesoporous silica materials, in: P. Ducheyne (Ed.), Comprehensive Biomaterials II, Elsevier, United Kingdom, 2017, pp. 644–685.

[42] S.A. Hassanzadeh-Tabrizi, A. Bigham, M. Rafienia, Surfactant assisted sol-gel synthesis of forsterite nano-particles as a novel drug delivery system, Mater. Sci. Eng. 58 (2016) 737–741, https://doi.org/10.1016/j.msec.2015.09.020.

[43] C.K. Lee, S.S. Liu, L.C. Juang, C.C. Wang, K.S. Lin, M.D.J. Lyu, Application of MCM-41 for dyes removal from wastewater, J. Hazard. Mater. 147 (3) (2007) 997–1005, https://doi.org/10.1016/j.jhazmat.2007.01.130.

[44] Z. Rahimi, A.A. Zinatizadeh, S. Zinadini, M. van Loosedrecht, H. Younesi, A new anti-fouling polysulphone nanofiltration membrane blended by amine-functionalized MCM-41 for post treating waste stabilization pond's effluent, J. Environ. Manag. 290 (2021) 112649, https://doi.org/10.1016/j.jenvman.2021.112649.

[45] B. Nohair, P.T.H. Thao, V.T.H. Nguyen, P.Q. Tien, D.T. Phuong, L.G. Hy, S. Kaliaguine, Hybrid Periodic Mesoporous Organosilicas (PMO-SBA-16): A Support for Immobilization of d-amino acid Oxidase and Glutaryl-7-amino Cephalosporanic acid Acylase Enzymes, J. Phys. Chem. C 116 (2012) 10904–10912, https://doi.org/10.1021/jp2116998.

[46] B. Zohra, K. Aicha, S. Fatima, B. Nourredine, D. Zoubir, Adsorption of direct red 2 on bentonite modified by cetyltrimethylammonium bromide, Chem. Eng. J. 136 (2008) 295–305, https://doi.org/10.1016/j.cej.2007.03.086.

[47] B.M. Estevao, I. Miletto, N. Hioka, L. Marchese, E. Gianotti, Mesoporous silica nanoparticles functionalized with amino groups for biomedical applications, ChemistryOpen 10 (12) (2021) 1251–1259, https://doi.org/10.1002/open.202100227.

[48] A. Saad, I. Bakas, J.-Y. Piquemal, S. Nowak, M. Abderrabba, M.M. Chehimi, Mesoporous silica/polyacrylamide composite: preparation by UVgraft photopolymerization, characterization and use as Hg (II) adsorbent, Appl. Surf. Sci. 367 (2016) 181–189, https://doi.org/10.1016/j.apsusc.2016.01.134.

[49] G. Yang, Y. Deng, H. Ding, Z. Lin, Y. Shao, Y. Wang, A facile approach to synthesize MCM-41 mesoporous materials from iron ore tailing: Influence of the synthesis conditions on the structural properties, Appl. Clay Sci. 3 (2015) 61–66, https://doi.org/10.1016/j.clay.2015.04.005.

[50] L. Han, C. Gao, X. Wu, Q. Chen, P. Shu, Z. Ding, S. Che, Anionic surfactants templating route for synthesizing silica hollow spheres with different shell porosity, Solid State Sci. 13 (2011) 721–728, https://doi.org/10.1016/j.solidstatesciences.2010.05.009.

[51] P. Ågren, M. Lindén, J.B. Rosenholm, R. Schwarzenbacher, M. Kriechbaum, H. Amenitsch, P. Laggner, J. Blanchard, F. Schüth, Kinetics of cosurfactant-surfactant-silicate phase behavior. 1. short-chain alcohols, J. Phys. Chem. B 103 (1999) 5943–5948, https://doi.org/10.1021/jp984684x.

[52] B. Boukoussa, Z. Kibou, Z. Abid, R. Ouargli, N. Choukchou-Braham, D. Villemin, A. Bengueddach, R. Hamacha, Key factor affecting the basicity of mesoporous silicas MCM-41: effect of surfactant extraction time and Si/Al ratio, Chem. Pap. 72 (2018) 289–299, https://doi.org/10.1007/s11696-017-0279-4.

[53] D.M. Oliveira, A.S. Andrada, Synthesis of ordered mesoporous silica MCM-41 with controlled morphology for potential application in controlled drug delivery

systems, Ceramica 65 (2019) 170–179, https://doi.org/10.1590/0366-69132019653742509.
[54] V. Cauda, A. Schlossbauer, J. Kecht, A. Zürner, T. Bein, Multiple core-shell functionalized colloidal mesoporous silica nanoparticles, J. Am. Chem. Soc. 131 (2009) 11361–11370, https://doi.org/10.1021/ja809346n.
[55] B.E.B. Costa, R.F. Damasceno, A.O.S. Siliva, S.M.P. Meneghetti, Characterisation of mesoporous stannosilicates obtained via non-hydrothermal synthesis using Na_2SnO_3 as the precursor, Microporous Mesoporous Mater. 310 (2021) 110630, https://doi.org/10.1016/j.micromeso.2020.110630.
[56] Y. Li, S. Li, Y. Kong, Hydroxylation of benzene to phenol over heteropoly acid $H_5PMo_{10}V_2O_{40}$ supported on amine-functionalised MCM-41, RSC Adv. 11 (2021) 26571–26580, https://doi.org/10.1039/D1RA04269F.
[57] P.D. Du, N.T. Hieu, T.C. To, L.G. Bach, M.X. Tinh, T.X. Mau, D.Q. Khieu, Aminopropyl functionalised MCM-41: synthesis and application for adsorption of Pb(II) and Cd(II), Adv. Mater. Sci. Eng. 2019 (2019) 8573451, https://doi.org/10.1155/2019/8573451.